Limit cycles in nonlinear vibrating systems excited by a nonideal energy source with a large slope characteristic

Javier González-Carbajal · Jaime Domínguez

Abstract This study is the natural continuation of a previous paper of the authors González-Carbajal and Domínguez in J. Sound Vib. (Under revision), where the possibility of finding Hopf bifurcations in vibrating systems excited by a nonideal power source was addressed. Herein, some analytical tools are used to characterize these Hopf bifurcations, deriving a simple rule to classify them as supercritical or subcritical. Moreover, we find conditions under which the averaged system can be proved to be always attracted by a limit cycle, irrespective of the initial conditions. These limit cycle oscillations in the averaged system correspond to quasiperiodic motions of the original system. To the authors' knowledge, limit cycle oscillations have not been addressed before in the literature about nonideal excitations. Through supporting numerical simulations, we also investigate the global bifurcations destroying the limit cycles. The analytical results are verified numerically.

Keywords Nonideal excitation · Unbalanced motor · Hopf bifurcation · Limit cycle

J. González-Carbajal (✉) · J. Domínguez
Department of Mechanical Engineering, University
of Seville, C/ Camino de los Descubrimientos s/n,
Isla de la Cartuja, 41092 Seville, Spain
e-mail: jgcarbajal@us.es

J. Domínguez
e-mail: jaime@us.es

1 Introduction

Vibrations caused by unbalanced rotating machinery are very frequently encountered in mechanical engineering [2,3]. This might be an undesired consequence of manufacturing errors and tolerances [4], which can endanger the performance of turbines, blowers, pumps, etc. On the other hand, there are also applications where rotors are purposely unbalanced to generate a useful vibration, as is the case of the feeding, conveying and screening of bulk materials or the vibrocompaction of quartz conglomerates.

In the analysis of these unbalance-induced oscillations, it is often necessary to take into account how the motion of the energy source is affected by vibration [5–8]. In these situations, where there is a significant two-way interaction between exciter and vibrating structure, the excitation is said to be nonideal.

The study of nonideal excitations begun with the experimental work of Sommerfeld [9]. He used a setup consisting in an unbalanced electric motor mounted on an elastically supported table, monitoring the input power and the amplitude and frequency of the response. Some anomalous phenomena were found, like jumps in the oscillation amplitude and ranges of frequency where no stationary motion could be obtained. These unexpected issues, known as 'the Sommerfeld effect', could not be explained by an ideal model, i.e. assuming that rotation was not affected by vibration.

Some years later, Kononenko [10] proposed an interpretation for the Sommerfeld effect, by considering a

model which included the nonideal coupling between motor and structure, and applying averaging techniques to the equations of motion. According to Kononenko, the Sommerfeld effect is due to the torque on the rotor produced by vibration of the unbalanced mass.

Rand et al. [11] reported the detrimental effect of a nonideal power source in dual-spin spacecrafts, which could endanger one of the manoeuvres of the spacecraft when placed in orbit.

Although the most usual analytical approach to the problem is based on averaging procedures, Blekhman proposed an alternative approximation to the stationary solutions by using the method of 'Direct Separation of Motions' [12].

El-Badawi [13] analysed a model where the vibrating structure had an intrinsic nonlinearity, in addition to the nonlinearity due to the nonideal coupling with the energy source.

For a more detailed exposition of the state of the art concerning nonideal systems, see [5].

A simple nonlinear mechanical system, excited by a nonideal unbalanced motor, was analytically and numerically studied in [1]. In that reference, thanks to a novel combination of two different perturbation techniques, the authors found conditions under which the system exhibited a Hopf bifurcation which had not been addressed before in the literature. This paper intends to be a direct continuation of [1], analysing in detail the appearance of Hopf bifurcations and their consequences.

It is well-known that Hopf bifurcations lead to the appearance of limit cycle oscillations (LCOs). Noticeably, the existence of LCOs as a consequence of nonidealness of the energy source has not been addressed before in the literature, to the best of the authors' knowledge.

The analytical study of bifurcations and limit cycles conducted in this paper, which is manageable for a 2D system, would be virtually unfeasible for a higher-dimensional system. As a matter of fact, the Poincaré–Bendixson (P–B) theorem, which is used herein to prove the existence of stable limit cycles, is only valid for 2D systems. These considerations suggest that the perturbation approach conducted in [1], which reduces the system dimension from 4 to 2, is particularly appropriate.

Finally, it is convenient to position the present paper within the literature, showing its similarities and differences with respect to other published works.

First, it should be noted that the Hopf bifurcation investigated in this paper is conceptually different to that reported in [14]. The reason is that while we study here the fixed points of an averaged system, representing stationary motions of the motor, Dantas et al. analysed in [14] the fixed points of the original system, corresponding to the motor at rest.

It should be stressed that the present paper is mainly based on analytical results, which are also validated by means of numerical simulations. This makes it significantly different to many other works, where conclusions are directly drawn from numerical experiments [15–17].

This paper studies a mechanical system which is very similar to that analysed by Fidlin in [18]. However, he considered a motor characteristic with small slope, while our assumption is the opposite. Actually, the slope of the motor characteristic curve is a chief parameter of the problem. The system exhibits different behaviours and requires different mathematical approaches, depending on the order of magnitude of this slope.

The mechanical system that we investigate is also akin to that studied by Rand et al. in [11,19]. However, they considered no damping and a motor driven by a constant torque. Due to these differences, both the perturbation approach and the conclusions about the motion of the system presented in this work are substantially different to those reported in [11,19].

There are also published works where chaotic behaviour is found in systems excited by nonideal power sources [17,20]. Nevertheless, this kind of motion is not possible for the particular case under study, as long as the assumptions specified in Sect. 2.1 hold. The reason is that at least 3 dimensions are needed to have chaos, while, as shown in Sect. 2.2, our reduced system is of dimension 2.

The organization of the paper is as follows. Section 2 briefly recalls the main results of [1], which constitute the base of this study. Section 3 analytically investigates conditions for the subcriticality or supercriticality of the Hopf bifurcations. Section 4 uses the Poincaré–Bendixson theorem to prove that, under appropriate conditions, every system trajectory is attracted by a limit cycle. The global bifurcations by means of which the limit cycles disappear are numerically investigated in Sect. 5. Section 6 compares numerical solutions of the reduced and the original system in order to validate the analytical developments and discusses the

timescale in which the asymptotic approximation is valid. Finally, the conclusions of the present study are summarized in Sect. 7.

2 Brief review of previous developments

2.1 Equations of motion and assumptions

Consider the system depicted in Fig. 1, consisting of an unbalanced motor attached to the fixed frame by means of a nonlinear spring—with linear and cubic components—and a linear damper.

Variable x represents the linear motion, ϕ is the angle of the rotor, m_1 is the unbalanced mass with eccentricity r, m_0 is the rest of the vibrating mass, I_0 is the rotor inertia (without including the unbalance), b is the damping coefficient and k and λ are, respectively, the linear and cubic coefficients of the spring. The equations of motion for the coupled 2-DOF system are

$$m\ddot{x} + b\dot{x} + kx + \lambda x^3 = m_1 r \left(\dot{\phi}^2 \cos \phi + \ddot{\phi} \sin \phi \right)$$
$$I\ddot{\phi} = L\left(\dot{\phi}\right) + m_1 r\ddot{x} \sin \phi, \tag{1}$$

where $m = m_0 + m_1$, $I = I_0 + m_1 r^2$. A dot represents differentiation with respect to time, t. Function $L\left(\dot{\phi}\right)$ is the driving torque produced by the motor—given by its static characteristic—minus the losses torque due to friction at the bearings, windage, etc. We assume this net torque to be a linear function of the rotor speed

$$L\left(\dot{\phi}\right) = C + D\left(\dot{\phi} - \omega_n\right), \tag{2}$$

where ω_n is the linear natural frequency of the oscillator, given by $\omega_n = \sqrt{k/m}$. Although $L\left(\dot{\phi}\right)$ includes the damping of rotational motion, we will usually refer
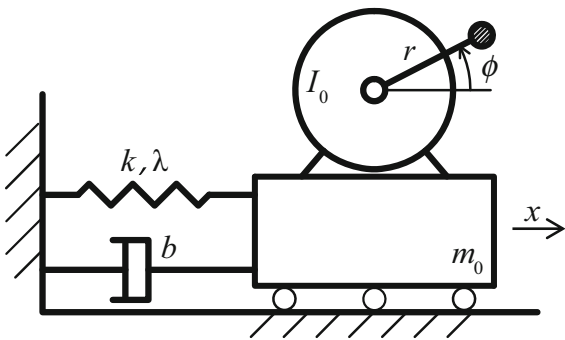

Fig. 1 Model of the mechanical system

to it shortly as '*the motor characteristic*'. We further assume $D < 0$—the driving torque decreases with the rotor speed—as is usual for most kinds of motor.

By defining

$$R_m = m_1/m, \quad R_I = m_1 r^2/I$$
$$\xi = \frac{b}{2\sqrt{km}}, \quad \alpha = \frac{R_I R_m}{2\xi}$$
$$c = \frac{C}{I\omega_n^2}, \quad d = \frac{D}{I\omega_n}, \quad \tau = \omega_n t$$
$$u = \frac{x}{r} \frac{2\xi}{R_m}, \quad \rho = \frac{\lambda r^2}{k} \left(\frac{R_m}{2\xi}\right)^2, \tag{3}$$

the equations of motion can be written in a more convenient dimensionless form

$$\ddot{u} + u = -2\xi\dot{u} - \rho u^3 + 2\xi \left(\dot{\phi}^2 \cos \phi + \ddot{\phi} \sin \phi\right)$$
$$\ddot{\phi} = c + d\left(\dot{\phi} - 1\right) + \alpha\ddot{u} \sin \phi, \tag{4}$$

where a dot now represents differentiation with respect to dimensionless time, τ.

In order to apply perturbation techniques to system (4), some assumptions on the order of magnitude of the system parameters have to be made. Thus, we assume the damping, the unbalance and the nonlinearity to be small. We express this by making the corresponding coefficients proportional to a sufficiently small, positive and dimensionless parameter ϵ:

$$\xi = \epsilon\xi_0, \quad \alpha = \epsilon\alpha_0, \quad \rho = \epsilon\rho_0. \tag{5}$$

We also assume that the torque generated by the motor at resonance $\left(\dot{\phi} = 1\right)$ is sufficiently small:

$$c = \epsilon c_0. \tag{6}$$

Finally, we assume the slope of the motor characteristic to be of the order of unity, i.e. independent of ϵ:

$$d = d_0. \tag{7}$$

This assumption corresponds to what we have called 'large slope characteristic'. The case of small slope, with d proportional to ϵ, is treated in [18].

Taking the proposed scaling (5)–(7) into account and dropping the subscript '0' for convenience, we can write (4) as

$$\ddot{u} + u = \epsilon \left\{ -2\xi\dot{u} - \rho u^3 + 2\xi \left(\dot{\phi}^2 \cos \phi + \ddot{\phi} \sin \phi\right) \right\}$$
$$\ddot{\phi} = d\left(\dot{\phi} - 1\right) + \{c + \alpha\ddot{u} \sin \phi\}. \tag{8}$$

In the next two subsections, we sketch some results obtained in [1] concerning the behaviour of (8), namely those which are necessary for the present paper.

2.2 Reduced system

Equation (8) constitutes an autonomous dynamical system of dimension 4, with state variables $\{u, \dot{u}, \phi, \dot{\phi}\}$. In Ref. [1], some perturbation techniques were applied to (8), in order render it easier to analyse. Here we mention the main results of this procedure:

- System (8) exhibits three qualitatively different behaviours, at three consecutive stages of time.
- The first two stages take place at a timescale $\tau = O(1)$. They can be considered as a fast transient regime.
- The third stage occurs at a timescale $\tau = O(1/\epsilon)$. During this stage, we have

$$\Omega \equiv \dot{\phi} = 1 + \epsilon\sigma, \tag{9}$$

which means that the system is near resonance.

- The system dynamics at the third stage is governed, with $O(\epsilon)$ precision, by the following 2D reduced model:

$$\left.\begin{array}{l} \dot{a} = -\epsilon\xi(a + \sin\beta) \\ \dot{\beta} = \epsilon\left(\frac{c}{d} + \frac{\alpha}{2d}a\sin\beta - \xi\frac{\cos\beta}{a} + \frac{3}{8}\rho a^2\right) \end{array}\right\}, \tag{10}$$

where the new variables are related to the original ones by

$$\left.\begin{array}{l} u = a\cos(\phi + \beta) \\ \dot{u} = -a\sin(\phi + \beta) \end{array}\right\}. \tag{11}$$

2.3 Equilibrium points and stability

Equilibrium points of system (10), which represent stationary solutions of the original system (8), can be obtained with the following graphical construction. Consider the plane spanned by axis $\{\sigma, T\}$, where σ is a measure of the rotor speed—see (9)—and T represents torque on the rotor. Graph T_m versus σ, with

$$T_m(\sigma) \equiv c + d\sigma. \tag{12}$$

Then, graph on the same plot the parametric curve given by $\{\sigma_v(z, a), T_v(a)\}$, with $z = \pm 1$, $a \in (0, 1]$ and
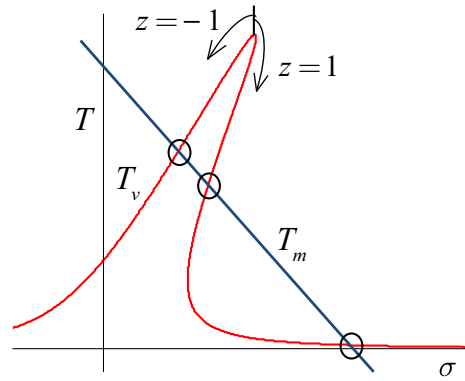

Fig. 2 Equilibrium points of (10)

$$\left.\begin{array}{l} T_v(a) \equiv \frac{\alpha}{2}a^2 \\ \sigma_v(z, a) \equiv \frac{3}{8}\rho a^2 + z\xi\frac{\sqrt{1-a^2}}{a} \end{array}\right\}. \tag{13}$$

The above procedure gives rise to a plot like that shown in Fig. 2, where the equilibrium points of (10) correspond to the intersections between the two curves. In the particular case displayed in Fig. 2, there are three equilibrium points, marked with circles. Note that curve T_v is composed of two branches, which collide at the maximum of the curve. They correspond to the two possible values of parameter z, as specified in Fig. 2.

The physical interpretation of Fig. 2 is as follows: T_m is the net torque produced by the motor, while T_v represents the torque on the rotor due to vibration.

For a particular intersection between the curves $\{\sigma_{eq}, T_{eq}\}$, the equilibrium values of $\{a, \beta\}$ are given by

$$a_{eq} = \sqrt{\frac{2T_{eq}}{\alpha}}, \quad \beta_{eq} = \tan^{-1}\left(\frac{-a_{eq}}{-zR_{eq}}\right), \tag{14}$$

where R_{eq} stands for $\sqrt{1 - a_{eq}^2}$.

Once the equilibrium points of the reduced system have been obtained, we turn to the analysis of their stability. For a 2D system, this reduces to calculating the trace and determinant of the Jacobian matrix, evaluated at the equilibrium point of interest:

$$J_{eq} = \epsilon\begin{bmatrix} -\xi & z\xi R_{eq} \\ \left(-\frac{\alpha}{2d} + \frac{3\rho}{4}\right)a_{eq} - \frac{z\xi R_{eq}}{a_{eq}^2} & -\frac{z\alpha a_{eq}R_{eq}}{2d} - \xi \end{bmatrix}, \tag{15}$$

The conditions for an equilibrium point to be asymptotically stable are

C1. $\text{tr}\left(J_{\text{eq}}\right) < 0$ (16)

C2. $\det\left(J_{\text{eq}}\right) > 0.$ (17)

After some algebra, these conditions can be expressed as

C1. $\dfrac{z\alpha a_{\text{eq}} R_{\text{eq}}}{4d} + \xi > 0$ (18)

C2. $\left\{ \begin{array}{l} \frac{1}{\eta} - \frac{1}{d} < 0, \ if \ z = 1 \\ \frac{1}{\eta} - \frac{1}{d} > 0, \ if \ z = -1 \end{array} \right\}$,   (19)

where η denotes the slope of the T_v curve at the considered equilibrium point and has expression

$$\frac{1}{\eta} = -\frac{z\xi}{\alpha a_{\text{eq}}^3 R_{\text{eq}}} + \frac{3\rho}{4\alpha}, \qquad (20)$$

as can be deduced from (13).

We now apply conditions (18) and (19) to evaluate stability regions in different scenarios. The procedure is as follows. Consider parameters α, ξ, ρ fixed, so that the T_v curve—see (13)—is fixed too. Consider a pair of values (c, d) which gives a particular curve $T_m(\sigma)$. The intersections between the two curves represent the equilibrium points of the system. Select one of them—if there are more than one—and let parameters (c, d) vary in such a way that the selected equilibrium point remains an equilibrium point. In other words, let parameters (c, d) vary so as to make the curve $T_m(\sigma)$ rotate around the selected equilibrium point, satisfying restriction $d < 0$. Finally, use conditions (18) and (19) to analyse how the stability of the equilibrium point is affected by the slope d of the motor characteristic.

The procedure described above was followed in [1] for all possible scenarios ($z = \pm 1$, $\eta \gtrless 0$); nonetheless, here we restrict attention to the only case of interest for the present paper, namely that exhibiting a Hopf bifurcation. Then, consider an equilibrium point satisfying

$$z = 1, \quad d_H < \eta < 0. \qquad (21)$$
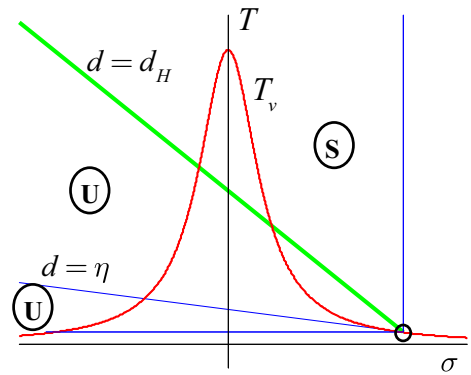
where critical slope d_H is defined as

Fig. 3 Stability regions for an equilibrium point exhibiting a Hopf bifurcation. S and U label the stable and unstable regions, respectively
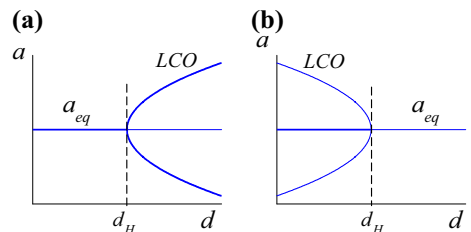

Fig. 4 Classification of Hopf bifurcations. **a** Supercritical, **b** subcritical. *Thick (thin) lines* represent stable (unstable) solutions

$$d_H\left(\alpha, \xi, a_{\text{eq}}\right) = -\frac{\alpha a_{\text{eq}} R_{\text{eq}}}{4\xi}. \qquad (22)$$

The stability diagram for this scenario is displayed in Fig. 3. The critical condition—i.e. the one which produces the stability change—is **C1**. In this case, the equilibrium point loses stability at $d = d_H$ through a Hopf bifurcation, after which we named parameter d_H.

3 Classification of the Hopf bifurcations

Clearly, it would be of great interest to characterize the Hopf bifurcation under study as subcritical or supercritical. In the former case, an unstable limit cycle coexists with the stable equilibrium point, while in the latter case there is a stable limit cycle coexisting with the unstable equilibrium point, as represented in Fig. 4. Subcritical bifurcations are generally more dangerous in real applications, since they can give rise to abrupt jumps in the system behaviour [21].

Characterizing the bifurcations require several transformations of system (10) that are detailed below.

3.1 Transformation to Cartesian coordinates

We assume the system parameters are such that there exists an equilibrium point satisfying condition (31) and, thereby, undergoing a Hopf bifurcation. By defining change of variables

$$\begin{cases} \tilde{x} = a\cos\beta \\ \tilde{y} = a\sin\beta \end{cases},$$
(23)

system (10) can be rewritten, at the bifurcation point ($d = d_H$), as

$$\begin{cases} \dot{\tilde{x}} = -\epsilon\left[\xi\tilde{x} + \frac{c}{d_H}\tilde{y} + \frac{\alpha}{2d_H}\tilde{y}^2 + \frac{3}{8}\rho\tilde{y}\left(\tilde{x}^2 + \tilde{y}^2\right)\right] \\ \dot{\tilde{y}} = \epsilon\left[-\xi - \xi\tilde{y} + \frac{c}{d_H}\tilde{x} + \frac{\alpha}{2d_H}\tilde{x}\tilde{y} + \frac{3}{8}\rho\tilde{x}\left(\tilde{x}^2 + \tilde{y}^2\right)\right] \end{cases}.$$
(24)

3.2 Displacement of the origin

In order to characterize the bifurcation, it is convenient to locate the origin of the coordinate system at the equilibrium point under investigation. Then, we define change of variables

$$\begin{cases} x = \tilde{x} - a_{\text{eq}}\cos\beta_{\text{eq}} \\ y = \tilde{y} - a_{\text{eq}}\sin\beta_{\text{eq}} \end{cases}.$$
(25)

Using the new coordinates, system (24) takes the form

$$\begin{cases} \dot{x} = \epsilon\left\{-\left[\xi + \frac{3}{4}\rho a^3 R\right]x - \left[\frac{3}{4}\rho a^4 + \xi\left(\frac{2a}{R} - \frac{R}{a}\right)\right]y + \frac{3}{8}\rho a^2 x^2 + \left[\frac{2\xi}{aR} + \frac{9}{8}\rho a^2\right]y^2 + \frac{3}{4}\rho aRxy - \frac{3}{8}\rho y\left[x^2 + y^2\right]\right\} \\ \dot{y} = \epsilon\left\{\left[\frac{3}{4}\rho a^2 R^2 - \xi\frac{R}{a}\right]x + \left[\xi + \frac{3}{4}\rho a^3 R\right]y - \frac{9}{8}\rho aRx^2 - \frac{3}{4}\rho aRy^2 - \left[\frac{2\xi}{aR} + \frac{3}{4}\rho a^2\right]xy + \frac{3}{8}\rho x\left[x^2 + y^2\right]\right\} \end{cases}$$
(26)

where a_{eq} and R_{eq} are shortly written as a and R, respectively, in order to make the expression more manageable. This abbreviated notation will also be used in equation (28) and in the "Appendix 1". Note that system (26) is of the form

$$\begin{Bmatrix} \dot{x} \\ \dot{y} \end{Bmatrix} = \epsilon\left\{A\begin{Bmatrix} x \\ y \end{Bmatrix} + h(x, y)\right\}$$
(27)

where matrix A is given by

$$A = \begin{bmatrix} -\left(\xi + \frac{3}{4}\rho a^3 R\right) & -\left\{\frac{3}{4}\rho a^4 + \xi\left(\frac{2a}{R} - \frac{R}{a}\right)\right\} \\ \frac{3}{4}\rho a^2 R^2 - \xi\frac{R}{a} & \xi + \frac{3}{4}\rho a^3 R \end{bmatrix}$$
(28)

and vector $h(x, y)$ contains the nonlinear terms of the system.

3.3 Transformation to the real eigenbasis of matrix A

We define a new change of variables using the real eigenbasis of matrix A:

$$\begin{Bmatrix} x \\ y \end{Bmatrix} = T\begin{Bmatrix} z_1 \\ z_2 \end{Bmatrix},$$
(29)

where the columns of matrix T are the real and imaginary parts of the complex conjugate eigenvectors of A, denoted by $v_{1,2}$:

$$v_{1,2} = \begin{Bmatrix} c_1 \\ c_2 \end{Bmatrix} \pm i\begin{Bmatrix} \omega_0 \\ 0 \end{Bmatrix} \rightarrow T = \begin{bmatrix} c_1 & \omega_0 \\ c_2 & 0 \end{bmatrix},$$
(30)

with

$$c_1 = \xi + \frac{3}{4}\rho a_{\text{eq}}^3 R_{\text{eq}}$$

$$c_2 = \xi\frac{R_{\text{eq}}}{a_{\text{eq}}} - \frac{3}{4}\rho a_{\text{eq}}^2 R_{\text{eq}}^2$$

$$\omega_0 = \sqrt{\left(\frac{1 - 4a_{\text{eq}}^2}{a_{\text{eq}}^2}\right)\xi^2 - \frac{3}{4}\rho\xi a_{\text{eq}} R_{\text{eq}}}.$$
(31)

System (26), written in terms of the new variables, takes the form

$$\begin{Bmatrix} \dot{z}_1 \\ \dot{z}_2 \end{Bmatrix} = \epsilon\left\{\begin{bmatrix} 0 & -\omega_0 \\ \omega_0 & 0 \end{bmatrix}\begin{Bmatrix} z_1 \\ z_2 \end{Bmatrix} + \begin{Bmatrix} f(z_1, z_2) \\ g(z_1, z_2) \end{Bmatrix}\right\},$$
(32)

where functions f and g, containing the nonlinear terms of the system, can be written as:

$$f(z_1, z_2) = \sum_{i+j=2}^{3} \frac{1}{i!j!}f_{ij}z_1^i z_2^j$$

$$g(z_1, z_2) = \sum_{i+j=2}^{3} \frac{1}{i!j!}g_{ij}z_1^i z_2^j$$
(33)

Coefficients f_{ij} and g_{ij} are specified in the Appendix.

3.4 Transformation to normal form

The final step to characterize the bifurcation includes transformation in complex form, near-identity transformation and transformation in polar coordinates [22].

This is a standard procedure whose details can be found in [21,23]. After these last transformations, system (32) can be written in its normal form

$$\dot{r} = \epsilon \delta r^3, \qquad (34)$$

which governs the radial dynamics at the bifurcation. As shown in [23], coefficient δ can be computed as

$$16\delta = \left\{ \begin{array}{l} f_{30} + f_{12} + g_{21} + g_{03} \\ + \frac{1}{\omega_0} \left[f_{11} (f_{20} + f_{02}) - g_{11} (g_{20} + g_{02}) \right] \\ + \frac{1}{\omega_0} \left[f_{02} g_{02} - f_{20} g_{20} \right] \end{array} \right\}. \qquad (35)$$

In summary, we can say that, after a large number of variable transformations, system (10) can be written as (34), from which we deduce that the bifurcation is supercritical (subcritical) if $\delta < 0$ ($\delta > 0$).

Despite the fact that coefficients f_{ij} and g_{ij} are of rather complicated form, we find—with the aid of software for symbolic computation—that the condition for supercriticality or subcriticality can be expressed in a surprisingly simple manner:

Supercrit. $\Rightarrow \delta < 0 \Rightarrow \rho < -\dfrac{8\xi}{3a_{eq}R_{eq}}$

Subcrit. $\Rightarrow \delta > 0 \Rightarrow \rho > -\dfrac{8\xi}{3a_{eq}R_{eq}}$ $\qquad (36)$

It is worth noting that conditions (36) admit a very clear graphical interpretation. Consider a curve T_m which intersects T_v at the equilibrium point under consideration and also at the *highest peak* of curve T_v. Let d_P denote the slope of this particular motor characteristic, as depicted in Fig. 5.

In order to obtain d_P, let us write the coordinates of the two points defining the straight line. First, the
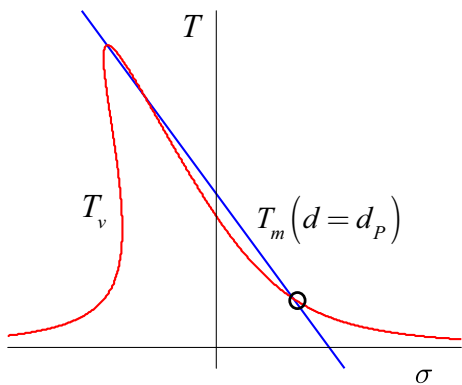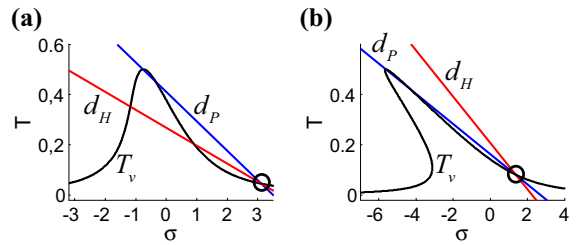

Fig. 5 Definition of slope d_P

Fig. 6 Examples of **a** subcritical and **b** supercritical bifurcations. **a** $\xi = 1$, $\alpha = 1$, $\rho = -2$, $a_{eq} = 0.3$, **b** $\xi = 1$, $\alpha = 1$, $\rho = -15$, $a_{eq} = 0.4$

highest peak of curve T_v can be shown to correspond to $a = 1$. Substituting this condition in (13), we obtain

$$\sigma = \frac{3}{8}\rho, \quad T = \frac{\alpha}{2} \qquad (37)$$

On the other hand, the (σ, T) coordinates of the equilibrium point under study are directly given in (13):

$$\sigma = \frac{3}{8}\rho a_{eq}^2 + \xi \frac{R_{eq}}{a_{eq}}, \quad T = \frac{\alpha}{2}a_{eq}^2 \qquad (38)$$

Then, from (37) and (38), the expression of d_P can be readily obtained:

$$\frac{1}{d_P} = \frac{3\rho}{4\alpha} - \frac{2\xi}{\alpha a_{eq}R_{eq}}, \qquad (39)$$

By comparing (39) and (22), conditions (36) can be expressed as

Supercritical $\Rightarrow d_H < d_P$

Subcritical $\Rightarrow d_H > d_P$. $\qquad (40)$

This last manner of characterizing the bifurcation is certainly appealing from a graphical point of view, since the basic information about the bifurcation can be directly observed from the torque–speed curves, as shown in Fig. 6 for two particular examples.

4 Conditions under which all system trajectories are attracted towards a limit cycle

In Sect. 3, a simple condition has been obtained to ascertain whether the Hopf bifurcation under study is subcritical or supercritical, which in turn allows predicting the kind of limit cycle generated by the bifurcation (see Fig. 4). Although this distinction is relevant, it is based on a local analysis and, consequently,

it only gives local information about the system behaviour. This is so in two senses: the analysis of Sect. 3 provides insight into the system dynamics

- for values of d close enough to d_H (results are local in the parameter space) and
- for trajectories close enough to the investigated equilibrium point (results are local in the phase plane).

In view of the aforementioned limitations, this section addresses a new global result that complements those of Sect. 3.

First, let us briefly recall the Poincaré–Bendixson theorem, which is an essential result from the global theory of nonlinear systems [24]. The theorem can be stated, in short terms, as follows.

Consider a 2D dynamical system and a closed, bounded region R of the phase plane which does not contain any equilibrium points. Then, every trajectory which is confined in R—it starts in R and remains in R for all future time—is a closed orbit or spirals towards a closed orbit as $t \to \infty$. For a more rigorous and detailed exposition of the theorem, see [24].

Let us show that, under certain circumstances, the P–B theorem can be used to prove that all trajectories of the system under study are attracted towards a limit cycle.

First, it can be easily deduced from (10) that

$$a > 1 \Rightarrow \dot{a} < 0. \tag{41}$$

Let us use variables a and β as polar coordinates on the phase plane, according to (13), and let D denote a circle centred at the origin of the phase plane with a radius slightly greater than 1; say 1.01. From (41), we can say that every trajectory starting outside region D will enter D and remain inside for all subsequent time. Obviously, trajectories starting inside D will also remain inside forever. This kind of behaviour would present D as a suitable candidate for the role of region R in the P–B theorem, if it were not for the presence of equilibrium points inside D.

Let us now consider the following particular situation:

$$\begin{cases} \text{The system has only one equilibrium point} \\ z = 1, \ \ d_H < d < \eta < 0 \end{cases} \tag{42}$$

whose torque curves are depicted in Fig. 7. We suppose that the only equilibrium point of the system is
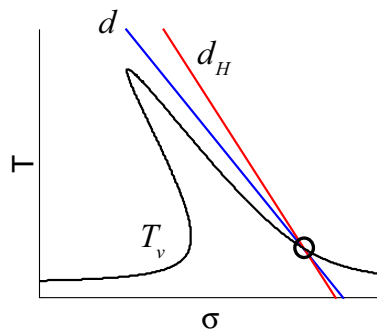

Fig. 7 Schematic view of the torque curves corresponding to conditions (42)

on the right branch of curve T_v and undergoes a Hopf bifurcation. It is also assumed that the actual slope of the motor characteristic is $d > d_H$ and, therefore, the equilibrium is unstable.

First, let us prove that the equilibrium point is a repeller. Since we already know that the equilibrium is unstable, we only need to prove that it is not a saddle. Let J_{eq} be the Jacobian matrix of system (10), evaluated at the equilibrium point. Taking into account that a saddle point has two real eigenvalues λ_1, λ_2 with different signs, we can state

$$\text{If } \det\left(J_{eq}\right) = \lambda_1 \lambda_2 > 0, \tag{43}$$

then the equilibrium is not a saddle.

With some simple algebra, it can be shown that, for $z = 1$, condition $\det\left(J_{eq}\right) > 0$ can be written as $d < \eta$. Then, it is clear that, for an equilibrium point satisfying (42), we have $\det\left(J_{eq}\right) > 0$. Thus, the equilibrium is a repeller.

Now, let us construct a new region Q, defined as D minus a circle of infinitesimal radius around the equilibrium point. From the above considerations—all trajectories enter D, and the equilibrium point is a repeller—it is clear that the flow on the boundary of Q is directed inwards, as depicted in Fig. 8.

In summary, we have obtained a closed, bounded region Q of the phase plane which contains no equilibrium points and such that all trajectories of the system enter Q and remain inside forever. Then, all conditions of the P–B theorem are fulfilled, and we can assure that any trajectory of the system is attracted towards a closed orbit as $t \to \infty$, if it is not a closed orbit itself.
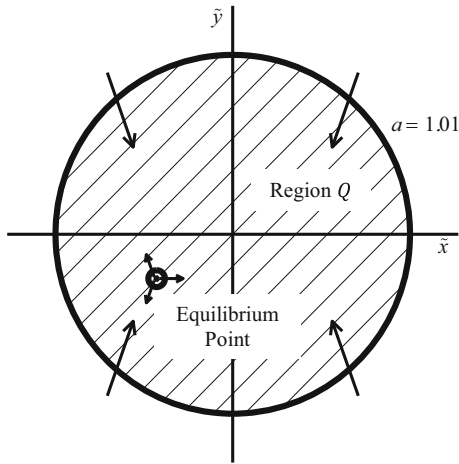
Fig. 8 Flow on the boundary of region Q (*dashed*), under conditions (42)

Finally, let us note that although the P–B theorem does not guarantee that all trajectories tend to the same closed orbit, all of our numerical simulations show the presence of only one stable limit cycle, namely that created by the Hopf bifurcation. This suggests that, for a system verifying (42), all the system dynamics is attracted towards a unique limit cycle.

5 Global bifurcations of the limit cycles

In Sect. 3, the creation of LCOs through Hopf bifurcations has been investigated. Now, we turn to the opposite question: once a limit cycle is born, does it exist for every $d > d_H$ in the supercritical case—for every $d < d_H$ in the subcritical case—or is it destroyed at any point? In the latter case, it would also be interesting to know the dynamical mechanism which makes the limit cycle disappear.

The aim of this section is to analyse the global dynamics of the system, tracking the evolution of the limit cycles in order to find out how they are destroyed—if they are destroyed at all. Since this task is in general too complex to be carried out analytically, we resort to numerical computation.

5.1 The subcritical case

Consider the following set of parameter values

$$\xi = 1, \quad \alpha = 1, \quad \rho = 0, \quad a_{\text{eq}} = 0.3, \quad z = 1. \quad (44)$$
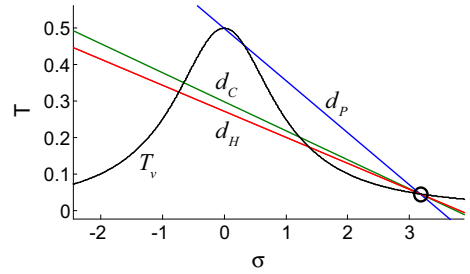

Fig. 9 Torque curves corresponding to parameters (44)

By using equations (22) and (39), we can obtain slopes d_H and d_P, depicted in Fig. 9.

$$d_H = -0.0715, \quad d_P = -0.1431 \quad (45)$$

According to criterion (40), the Hopf bifurcation is found to be subcritical. Thus, as represented in Fig. 4, an unstable limit cycle is known to exist for $d < d_H$, within a certain neighbourhood of d_H. We are interested in tracking the evolution of this limit cycle as slope d decreases. By numerically integrating system (10), through a Runge–Kutta algorithm, for different values of d, the limit cycle is found to disappear at $d = d_C$—see Fig. 9—with

$$d_C = -0.0795. \quad (46)$$

The dynamical mechanism whereby the limit cycle is destroyed, which turns out to be a homoclinic bifurcation [21], is shown in Fig. 10. Let us follow the evolution of the phase portrait. From Fig. 10a to Fig. 10b, the Hopf bifurcation takes place: the focus becomes stable, while an unstable limit cycle is born around it. In Fig. 10c, the cycle has swelled considerably and passes close to saddle point S. The homoclinic bifurcation occurs when the cycle touches the saddle point ($d = d_C$), becoming a homoclinic orbit. In Fig. 10d, we have $d < d_C$ and the loop has been destroyed.

It is worth noting that when the unstable limit cycle exists—namely for $d_C < d < d_H$—it acts as a frontier between the domains of attraction of the two stable equilibrium points of the system—see Fig. 10b, c.

Many other cases exhibiting a subcritical bifurcation, which are not shown here, have also been numerically solved. In all of them, the unstable limit cycle has been found to disappear through a homoclinic bifurcation.
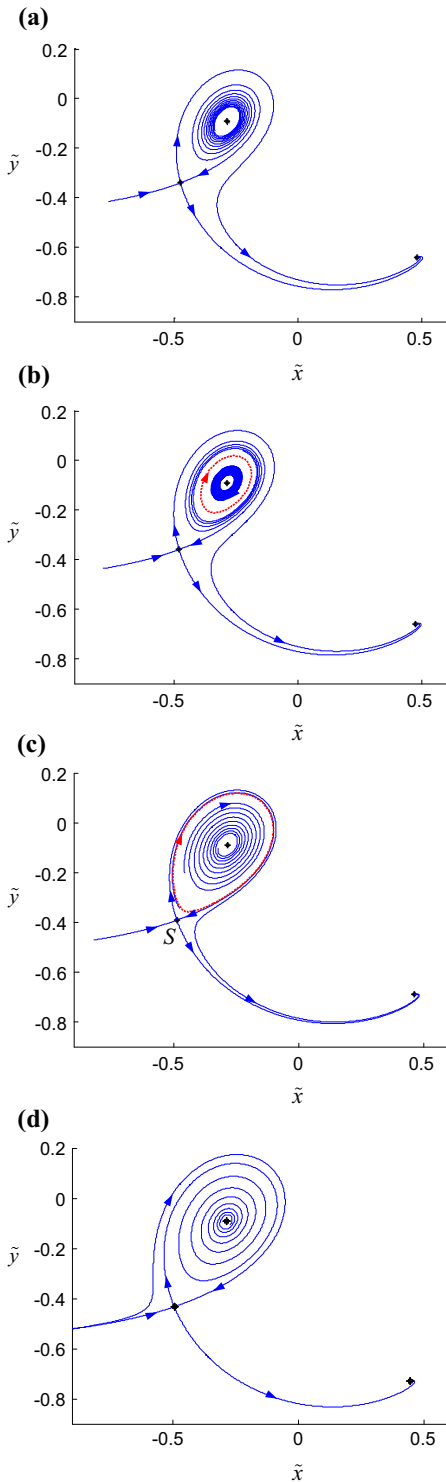
Fig. 10 Phase portraits corresponding to parameters (44). The equilibrium points are marked with *stars*. The *dashed loop* represents the unstable limit cycle. **a** $d = -0.070$, **b** $d = -0.073$, **c** $d = -0.078$, **d** $d = -0.081$
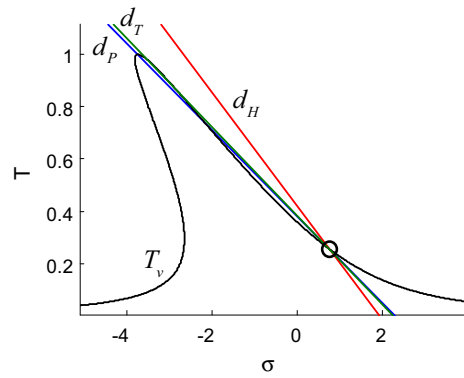
Fig. 11 Torque curves corresponding to parameters (47)

5.2 The supercritical case

Consider the following set of parameters:

$$\xi = 1, \quad \alpha = 2, \quad \rho = -10, \quad a_{eq} = 0.5, \quad z = 1. \tag{47}$$

Equations (22) and (39) yield the values of slopes d_H and d_P, depicted in Fig. 11.

$$d_H = -0.2165, \quad d_P = -0.1650 \tag{48}$$

Criterion (40) allows characterizing the bifurcation as supercritical. Then, as represented in Fig. 4, we can assure that a stable limit cycle encircles the unstable equilibrium for $d > d_H$, within a certain neighbourhood of d_H. As a matter of fact, the results of Section 4 can be used here to investigate the range of slopes d for which the limit cycle exists.

Consider the curve T_m which intersects T_v at the equilibrium point under study and is *tangent* to curve T_v at another point. Let d_T stand for the slope of that particular torque curve, as displayed in Fig. 11. Then, it is straightforward to show that, for $d_H < d < d_T$, conditions (42) are fulfilled and, consequently, we can assure that all system trajectories tend to a periodic orbit. In the case under analysis, we have

$$d_T = -0.1697. \tag{49}$$

Note that the Poincaré–Bendixson theorem gives sufficient, but not necessary, conditions for the existence of a stable periodic orbit. Thus, we cannot deduce from the theorem whether the limit cycle survives or not when

$d > d_T$. To the end of answering this question, we resort again to a numerical resolution of system (10), for increasing values of d. The results are displayed in Fig. 12.

Let us track the evolution of the phase portrait. In Fig. 12a, we have $d < d_H$ and all system trajectories are attracted towards the only equilibrium point of the system. Figure 12b corresponds to $d_H < d < d_T$. The Hopf bifurcation has occurred and, therefore, the focus has lost its stability at the same time that a stable limit cycle has appeared around it. Note that, in Fig. 12b, conditions (42) hold. Consequently, all system trajectories are attracted towards a periodic orbit. This scenario belongs to the general picture shown in Fig. 8.

The numerical results mentioned above are only useful to confirm the analytical developments of previous sections. By contrast, Fig. 12c does provide new information about the global dynamics of the system. It shows that the stable limit cycle is destroyed through a saddle-node homoclinic bifurcation [21], which occurs at $d = d_T$. This means that the cycle disappears exactly when conditions (42) are not fulfilled anymore. The mechanism is as follows. At $d = d_T$, a new equilibrium point, which immediately splits into a saddle and a node, is created through a saddle-node bifurcation. This new equilibrium appears precisely on the limit cycle, transforming it into a homoclinic orbit. What we find at $d > d_T$, as observed in Fig. 12c, is that the limit cycle has been replaced by a couple of heteroclinic orbits connecting the saddle and the node.

We have found that, for the particular set of parameters (47), conditions (42) are necessary and sufficient for the existence of a stable limit cycle. Thus, the periodic orbit never coexists with any other attractor of the system. Nevertheless, it should be stressed that this is not always the case. In fact, we have also found cases where the stable limit cycle is destroyed through a homoclinic bifurcation, just like in the subcritical case. In these situations, the global bifurcation occurs at certain slope $d_C > d_T$ and, therefore, the limit cycle coexists with a stable equilibrium for $d_T < d < d_C$.

As an example, consider a case with d_H satisfying $d_T < d_H < d_P$. Clearly, according to (40), the Hopf bifurcation is supercritical. However, it is not possible for the limit cycle to be destroyed through a saddle-node homoclinic bifurcation, because the saddle and the node are created before the limit cycle. In fact, in these cases, we have found the closed orbit to die in the
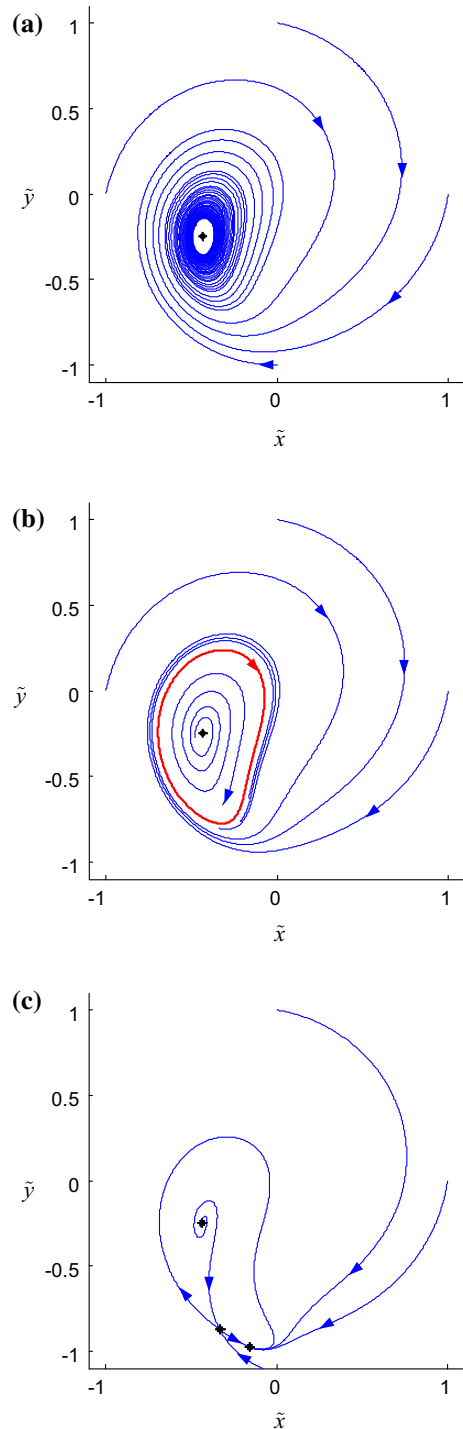

Fig. 12 Phase portraits corresponding to parameters (47). The equilibrium points are marked with stars. The *solid loop* represents the stable limit cycle **a** $d = -0.22$, **b** $d = -0.19$, **c** $d = -0.169$

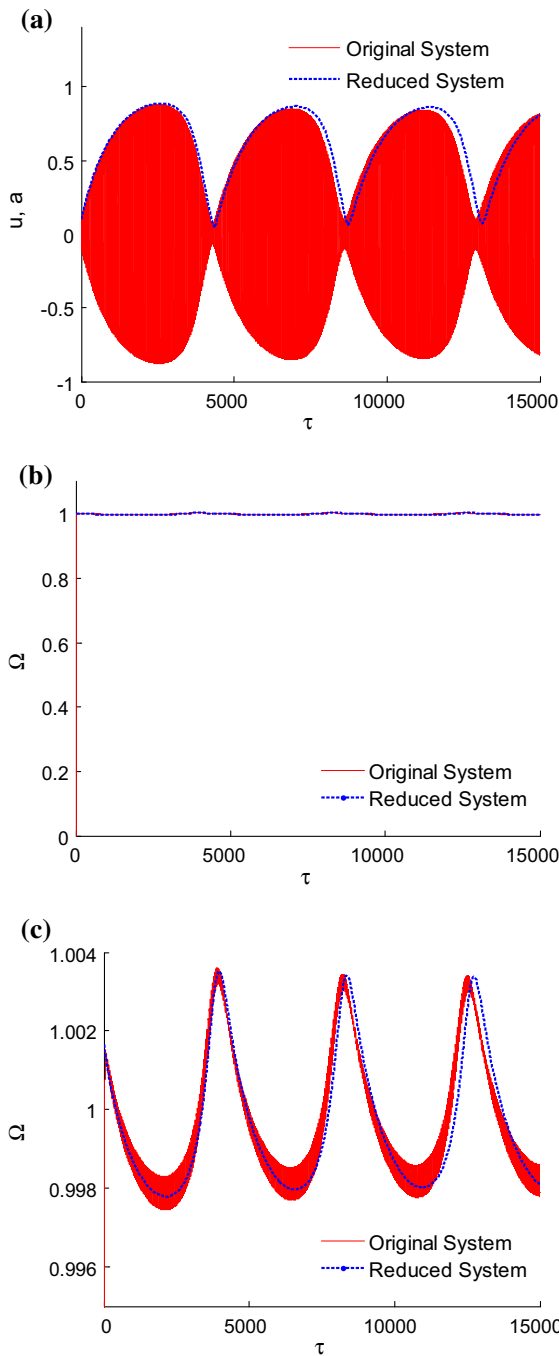**(a)**

(b)

(c)

Fig. 13 Comparison of numerical solutions of the original and reduced systems for parameters (47) and $d = -0.19$. **a** Displacement, **b** rotor speed (full view), **c** rotor speed (close-up around resonance)

same way as the unstable limit cycle shown in Fig. 10, i.e. through a homoclinic bifurcation due to the presence of a saddle point.

In summary, the simulations carried out suggest that, while unstable limit cycles are destroyed by homoclinic bifurcations, the stable ones can disappear either through homoclinic bifurcations or saddle-node homoclinic bifurcations.

6 Numerical validation and discussion

All the analytical and numerical analysis carried out thus far has dealt with the behaviour of system (10). Nonetheless, it should be recalled that (10) represents the reduced system, i.e. an asymptotic approximation to the original system (8). Thus, it would be convenient to verify whether the obtained results hold also for the original system. The aim of this section is to compare numerical solutions of the original and reduced systems in order to validate the proposed approach.

Consider again the set of parameters given at (47) and a motor characteristic with slope $d = -0.19$, which corresponds to the phase portrait exhibited in Fig. 12b. With these parameters, the original system of equation (8) is numerically solved for $\epsilon = 0.001$ and initial conditions

$$\left\{ \begin{array}{l} u_0 = 0.1 \\ \dot{u}_0 = 0 \\ \phi_0 = 0 \\ \dot{\phi}_0 = 0 \end{array} \right\}. \tag{50}$$

The reduced system (10) is numerically integrated as well for comparison. As explained in [1], the initial conditions for the original system $\{u_0, \dot{u}, \phi_0, \dot{\phi}_0\}$ and those for the reduced systems $\{a_0, \beta_0^*\}$ are related by

$$\begin{array}{l} a_0 = \sqrt{u_0^2 + \dot{u}_0^2} \\ \beta_0^* = \tan^{-1}\left(\dfrac{-\dot{u}_0}{u_0}\right) - \phi_0 + \dfrac{\dot{\phi}_0 - 1}{d}. \end{array} \tag{51}$$

Introducing (50) in (51) yields

$$\{a_0 = 0.1, \beta_0^* = 5.263\}. \tag{52}$$

With these sets of initial conditions, the obtained results for both systems are represented in Fig. 13, exhibiting very good agreement.

It is worth stressing that, as depicted in Fig. 13, a new kind of behaviour has been found for the mechanical system under study, which consists in a vibratory motion of the structure with slowly oscillating amplitude, due to the nonideal interaction between exciter and vibrating system. The periodic solutions of the

averaged system correspond to quasiperiodic solutions of the original one.

This type of motion had not been addressed before, to the authors' knowledge, in the literature about non-ideal excitations. Note that the LCOs give rise, in this case, to very large variations of the amplitude. Thus, the effect of the studied instability may be of great importance in real applications.

We also perform numerical validation of the results concerning subcritical Hopf bifurcations. To this end, consider again parameters (44) and a slope of the motor characteristic $d = -0.078$, which corresponds to the phase portrait displayed in Fig. 10c. In this scenario, as pointed out in Sect. 5.1, the unstable limit cycle is the boundary which separates the basins of attraction of the two attracting equilibrium points present in the system.

Two sets of initial conditions, I.C. (1) and I.C. (2), are selected, outside and inside the limit cycle, respectively:

$$\text{I.C. (1)} \begin{Bmatrix} a_0 = 0.1 \\ \beta_0^* = -2.8 \end{Bmatrix}, \quad \text{I.C. (2)} \begin{Bmatrix} a_0 = 0.2 \\ \beta_0^* = -2.8 \end{Bmatrix}. \tag{53}$$

Then, by using relations (51), we can compute corresponding initial conditions for the original system:

$$\text{I.C. (1)} \begin{Bmatrix} u_0 = 0.1 \\ \dot{u}_0 = 0 \\ \phi_0 = 2.8 \\ \dot{\phi}_0 = 1 \end{Bmatrix}, \quad \text{I.C. (2)} \begin{Bmatrix} u_0 = 0.2 \\ \dot{u}_0 = 0 \\ \phi_0 = 2.8 \\ \dot{\phi}_0 = 1 \end{Bmatrix}. \tag{54}$$

Note that this step has not a unique solution, because different sets of original initial conditions can produce the same reduced initial conditions.

The obtained numerical solutions are shown in Fig. 14, for $\epsilon = 0.001$. A good agreement between solutions of both systems is observed. Clearly, the two considered sets of initial conditions lead the system to different attractors.

Finally, it is convenient to consider the timescale in which the considered solutions of the reduced system are valid, which is a critical point in any perturbation analysis. It was shown in [1] that this time validity is, at least, $\tau = O(1/\epsilon)$. In fact, for the stable LCOs considered in this paper, we have an even stronger result. From the averaging theory, it is known that a solution of the averaged system which tends to an asymptotically stable periodic orbit is valid on $\tau \in [0, \infty)$ for
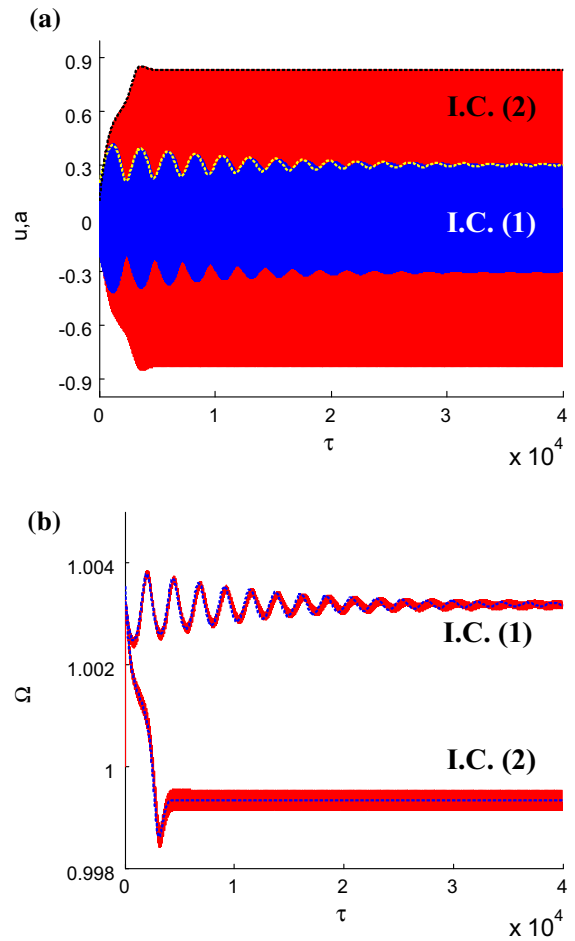

Fig. 14 Comparison of numerical solutions of the original (*solid line*) and reduced (*dashed line*) systems for parameters (44) and $d = -0.078$. **a** Displacements, **b** rotor speed

all variables except the angular one, i.e. the variable which measures the flow on the closed orbit [25]. This is equivalent to saying that we can uniformly approximate the closeness to the limit cycle, but not the position on it. The reason is that any small deviation on the frequency is accumulated over the cycles, giving rise to large errors after a sufficient number of periods (see Fig. 13).

7 Conclusions

This paper is concerned with the analytical and numerical analysis of a nonlinear mechanical system, excited by an unbalanced motor. The main contributions of the present study are summarized as follows.

- The Hopf bifurcations found in [1] have been analytically investigated, in order to characterize them as subcritical or supercritical. A very simple criterion, with clear graphical interpretation, has been obtained to distinguish both types of bifurcations.
- The Poincaré–Bendixson theorem has been used to find conditions under which all trajectories in the averaged system are attracted towards a periodic orbit, corresponding to a quasiperiodic solution of the original system.
- The global bifurcations destroying the stable and unstable limit cycles have been numerically investigated. These simulations suggest that unstable LCOs are destroyed through homoclinic bifurcations, while stable LCOs can be destroyed either through homoclinic bifurcations or through saddle-node homoclinic bifurcations.
- When there exists an unstable limit cycle, the system exhibits two stable equilibrium points, whose domains of attraction are clearly delimited by the periodic orbit.
- The presence of LCOs in the problem under study has been confirmed by numerically solving the original system of equations. An excellent agreement between the solutions of the original and reduced systems has been found. In addition, numerical results show that LCOs can produce very significant variations in the vibration amplitude, which suggests that the addressed instability might be of great relevance in real applications.

Appendix 1: coefficients f_{ij} and g_{ij}

The coefficients of functions $f(z_1, z_2)$ and $g(z_1, z_2)$ in (33) have the following expressions.

$$f_{20} = -\frac{3\rho aR}{4c_2}\left(3c_1^2 + c_2^2\right) - 2c_1\left(\frac{2\xi}{aR} + \frac{3}{4}\rho a^2\right) \tag{55}$$

$$f_{02} = -\frac{9\rho aR\omega_0^2}{4c_2} \tag{56}$$

$$f_{11} = -\frac{3}{4}\rho\omega_0 a\left(a + 3R\frac{c_1}{c_2}\right) - \frac{2\xi\omega_0}{aR} \tag{57}$$

$$f_{30} = \frac{9\rho c_1}{4c_2}\left(c_1^2 + c_2^2\right) \tag{58}$$

$$f_{03} = \frac{9\rho\omega_0^3}{4c_2} \tag{59}$$

$$f_{21} = \frac{3\rho\omega_0}{4c_2}\left(3c_1^2 + c_2^2\right) \tag{60}$$

$$f_{12} = \frac{9c_1\rho\omega_0^2}{4c_2} \tag{61}$$

$$g_{20} = \frac{(c_1^2 + c_2^2)}{\omega_0}\left\{\frac{9\rho a}{4}\left(R\frac{c_1}{c_2} + a\right) + \frac{4\xi}{aR}\right\} \tag{62}$$

$$g_{02} = \frac{3\rho\omega_0 a}{4}\left(a + 3R\frac{c_1}{c_2}\right) \tag{63}$$

$$g_{11} = \frac{3}{2}\rho a^2 c_1 + \frac{3\rho aR}{4c_2}\left(3c_1^2 + c_2^2\right) + \frac{2\xi c_1}{aR} \tag{64}$$

$$g_{30} = -\frac{9\rho}{4\omega_0 c_2}\left(c_1^2 + c_2^2\right)^2 \tag{65}$$

$$g_{03} = -\frac{9c_1\rho\omega_0^2}{4c_2} \tag{66}$$

$$g_{21} = -\frac{9c_1\rho}{4c_2}\left(c_1^2 + c_2^2\right) \tag{67}$$

$$g_{12} = -\frac{3\rho\omega_0}{4c_2}\left(3c_1^2 + c_2^2\right) \tag{68}$$

where a_{eq} and R_{eq} have been shortly written as a and R, respectively.

References

1. González-Carbajal, J., Domínguez, J.: Nonlinear vibrating systems excited by a nonideal energy source with a large slope characteristic. J. Sound Vib. (Under revision)
2. Abbasi, A., Khadem, S.E., Bab, S., Friswell, M.I.: Vibration control of a rotor supported by journal bearings and an asymmetric high-static low-dynamic stiffness suspension. Nonlinear Dyn. **85**(1), 525–545 (2016)
3. Boyaci, A., Lu, D., Schweizer, B.: Stability and bifurcation phenomena of Laval/Jeffcott rotors in semi-floating ring bearings. Nonlinear Dyn. **79**, 1535–1561 (2015)
4. Shabana, A.A.: Theory of Vibration (an introduction). Springer, New York (1996). doi:10.1007/978-1-4612-3976-5
5. Balthazar, J.M., Mook, D.T., Weber, H.I., R, B., Fenili, A., Belato, D., Felix, J.L.P.: An Overview on non-ideal vibrations. Meccanica **38**, 613–621 (2003)
6. Munteanu, L., Chiroiu, V., Sireteanu, T.: On the response of small buildings to vibrations. Nonlinear Dyn. **73**, 1527–1543 (2013)
7. Dimentberg, M.F., Mcgovern, L., Norton, R.L., Chapdelaine, J., Harrison, R.: Dynamics of an unbalanced shaft interacting with a limited power supply. Nonlinear Dyn. **13**(2), 171–187 (1997)

8. Awrejcewicz, J., Starosta, R., Sypniewska-Kamińska, G.: Decomposition of governing equations in the analysis of resonant response of a nonlinear and non-ideal vibrating system. Nonlinear Dyn. **82**, 299–309 (2015)
9. Sommerfeld, A.: Naturwissenchftliche Ergebnisse der Neuren Technischen Mechanik. Verein Dtsch. Ing. Zeitscchrift **18**, 631–636 (1904)
10. Kononenko, V.O.: Vibrating Systems with a limited power supply. Illife, London (1969)
11. Rand, R.H., Kinsey, R.J., Mingori, D.L.: Dynamics of spinup through resonance. Int. J. Non Linear. Mech. **27**, 489–502 (1992)
12. Blekhman, I.I.: Vibrational Mechanics-Nonlinear Dynamic Effects. General Approach. World Scientific, Singapore (2000)
13. El-Badawy, A.A.: Behavioral investigation of a nonlinear nonideal vibrating system. J. Vib. Control **13**, 203–217 (2007)
14. Dantas, M.J.H., Balthazar, J.M.: On the appearance of a Hopf bifurcation in a non-ideal mechanical problem. Mech. Res. Commun. **30**, 493–503 (2003)
15. Felix, J.L.P., Balthazar, J.M.: Comments on a nonlinear and nonideal electromechanical damping vibration absorber, Sommerfeld effect and energy transfer. Nonlinear Dyn. **55**, 1–11 (2009)
16. Felix, J.L.P., Balthazar, J.M., Dantas, M.J.H.: On energy pumping, synchronization and beat phenomenon in a nonideal structure coupled to an essentially nonlinear oscillator. Nonlinear Dyn. **56**, 1–11 (2009)
17. Krasnopolskaya, T.S., Shvets, A.Y.: Chaos in vibrating systems with a limited power-supply. Chaos **3**, 387–395 (1993)
18. Fidlin, A.: Nonlinear Oscillations in Mechanical Engineering. Springer, Berlin (2006)
19. Quinn, D., Rand, R., Bridge, J.: The dynamics of resonant capture. Nonlinear Dyn. **8**, 1–20 (1995)
20. Belato, D., Weber, H.I., Balthazar, J.M., Mook, D.T.: Chaotic vibrations of a nonideal electro-mechanical system. Int. J. Solids Struct. **38**, 1699–1706 (2001)
21. Kuznetsov, Y.A.: Elements of Applied Bifurcation Theory. 2nd edn. Springer, New York (1998)
22. Habib, G., Kerschen, G.: Suppression of limit cycle oscillations using the nonlinear tuned vibration absorber. Proc. R. Soc. A **471**, 20140976 (2015). doi:10.1098/rspa.2014.0976
23. Guckenheimer, J., Holmes, P.: Nonlinear Oscillations, Dynamical Systems, and Bifurcations of Vector Fields. Springer, New York (1983)
24. Perko, L.: Differential Equations and Dynamical Systems, 3rd edn. Springer, New York (2001)
25. Sanders, J.A., Verhulst, F.: Averaging Methods in Nonlinear Dynamical Systems. Springer, New York (2007)